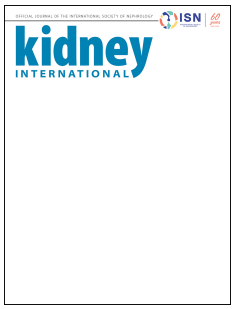

Hyperphosphatemia in chronic kidney disease exacerbates atherosclerosis via a mannosidases-mediated complex-type conversion of SCAP N-glycans.

Chao Zhou, MD, PhD, Quan He, MD, PhD, Hua Gan, MD, Tingting Zeng, MD, Qiao Liu, MD, PhD, John F. Moorhead, MD, Zac Varghese, MD, PhD, Nan Ouyang, MD, Xiong Z. Ruan, PhD

PII: S0085-2538(21)00188-5

DOI: https://doi.org/10.1016/j.kint.2021.01.016

Reference: KINT 2481

To appear in: *Kidney International*

Received Date: 29 March 2020

Revised Date: 4 January 2021

Accepted Date: 12 January 2021

Please cite this article as: Zhou C, He Q, Gan H, Zeng T, Liu Q, Moorhead JF, Varghese Z, Ouyang N, Ruan XZ, Hyperphosphatemia in chronic kidney disease exacerbates atherosclerosis via a mannosidases-mediated complex-type conversion of SCAP N-glycans., *Kidney International* (2021), doi: https://doi.org/10.1016/j.kint.2021.01.016.

Hyperphosphatemia in chronic kidney disease exacerbates atherosclerosis via a mannosidases-mediated complex-type conversion of SCAP N-glycans.

Chinese CKD population

438 patients

Radial arteries of uremic patients

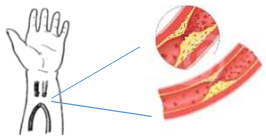

Hyperphosphatemic Apo-E -/- mice

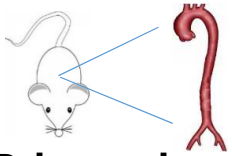

Primary human aortic smooth muscle cells

Hyperphosphatemia, an independent risk factor for atherosclerotic cardiovascular disease (ASCVD) in China

(***Cross-sectional study***)

Elucidation of mechanism involved in the acceleration of atherosclerosis by hyper-phosphatemia in CKD patients

Increase in ASCVD risk with rising serum phosphate levels

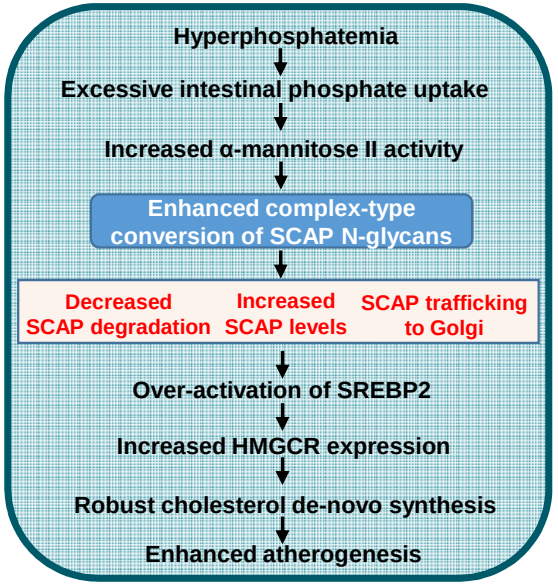

SCAP/SREBP2,cleavage-activating protein/ sterol regulatory element-binding protein

CONCLUSION:

Hyperphosphatemia increases cellular α-mannitose II activity and cholesterol synthesis via enhanced SCAP/SREBP2 signaling and modulation of SCAP N-glycans.

ISN kidney INTERNATIONAL
OFFICIAL JOURNAL OF THE INTERNATIONAL SOCIETY OF NEPHROLOGY

Zhou et al, 2021

[QUERY TO AUTHOR: title and abstract rewritten by Editorial Office - not subject to change]

Hyperphosphatemia in chronic kidney disease exacerbates atherosclerosis via a mannosidases-mediated complex-type conversion of SCAP N-glycans.

Chao Zhou[1], MD, PhD; Quan He[1], MD, PhD; Hua Gan[2], MD; Tingting Zeng[1], MD; Qiao Liu[1], MD, PhD; John F. Moorhead[3], MD; Zac Varghese[3], MD, PhD; Nan Ouyang[2]*, MD; Xiong Z Ruan[3,4]*, PhD;

[1] Department of Cardiology, The First Affiliated Hospital of Chongqing Medical University, Chongqing, PR. China, 400016;

[2] Department of Nephrology, The First Affiliated Hospital of Chongqing Medical University, Chongqing, PR. China, 400016;

[3] John Moorhead Research Laboratory, Centre for Nephrology, University College London (UCL) Medical School, Royal Free Campus, London, United Kingdom, NW32PF;

[4] Centre for Lipid Research & Key Laboratory of Molecular Biology for Infectious Diseases (Ministry of Education), Institute for Viral Hepatitis, Department of Infectious Diseases, the Second Affiliated Hospital, Chongqing Medical University, Chongqing, PR. China, 400016.

Running title: Hyperphosphatemia accelerates ASCVD.

Address Correspondence To:

Dr. Nan Ouyang and Xiong Z. Ruan, Department of Nephrology, The First Affiliated Hospital of Chongqing Medical University, Chongqing, P.R. China, 400016. E-mail: ouyangnan930@hotmail.com or x.ruan@ucl.ac.uk. Tel: 86-13594219877.

Funding: This work was supported by National Key R&D Program of China (2018YFC1312700), National Natural Science Foundation of China (NO. 81500341, NO. 81900406), Chongqing Science & Technology Commission (NO. cstc2018jcyjAX0134, NO. cstc2020jcyj-msxmX0304, NO. cstc2020jcyj-msxmX0152) and Moorhead Trust.

Abstract

Blood phosphate levels are linked to atherosclerotic cardiovascular disease in patients with chronic kidney disease (CKD), but the molecular mechanisms remain unclear. Emerging studies indicate an involvement of hyperphosphatemia in CKD accelerated atherogenesis through disturbed cholesterol homeostasis. Here, we investigated a potential atherogenic role of high phosphate concentrations acting through aberrant activation of sterol regulatory element-binding protein (SREBP) and cleavage-activating protein (SCAP)-SREBP2 signaling in patients with CKD, hyperphosphatemic apolipoprotein E (ApoE) knockout mice, and cultured vascular smooth muscle cells. Hyperphosphatemia correlated positively with increased atherosclerotic cardiovascular disease risk in Chinese patients with CKD and severe atheromatous lesions in the aortas of ApoE knockout mice. Mice arteries had elevated SCAP levels with aberrantly activated SCAP-SREBP2 signaling. Excess phosphate *in vitro* raised the activity of α-mannosidase, resulting in delayed SCAP degradation through promoting complex-type conversion of SCAP N-glycans. The retention of SCAP enhanced transactivation of SREBP2 and expression of 3-hydroxy-3-methyl-glutaryl coenzyme A reductase, boosting intracellular cholesterol synthesis. Elevated α-mannosidase II activity was also observed in the aortas of ApoE knockout mice and the radial arteries of patients with uremia and hyperphosphatemia. High phosphate concentration in vitro elevated α-mannosidase II activity in the Golgi, enhanced complex-type conversion of SCAP N-glycans, thereby upregulating intracellular cholesterol synthesis. Thus, our studies explain how hyperphosphatemia independently accelerates atherosclerosis in CKD.

Keywords: Hyperphosphatemia; SCAP N-glycans conversion; HMGCR; Atherosclerosis; α-Mannosidase activity

Translational Statement

Hyperphosphatemia accelerates atherosclerotic cardiovascular disease (ASCVD), but the underlying mechanisms are still unclear. This paper describes a new mechanism by which hyperphosphatemia increased the activity of α-mannosidase II in the Golgi, which enhanced sterol regulatory element-binding protein (SREBP) cleavage-activating protein (SCAP) mediated SREBP2 activation in lipid synthesis by modulating SCAP N-glycans. Our work provides a mechanistic explanation for a high incidence of ASCVD in CKD patients and the underlying mechanisms by which phosphate directly affecting vessel lipid homeostasis without changing blood lipid levels. It may also contribute to the design of effective dual therapeutic strategies targeting both phosphate and lipid metabolisms in the CKD population.

Introduction

Atherosclerotic cardiovascular disease (ASCVD) is the leading cause of mortality in patients with chronic kidney disease (CKD).[1] Cholesterol blood levels in CKD patients are usually normal or even low but are associated with extraordinarily high ASCVD risk.[2] This clinical phenomenon implies that cholesterol metabolism in CKD patients differs from that of the general population, and that non-classical risk factors may disrupt lipid homeostasis in CKD to significantly increase ASCVD by unknown mechanisms.[2-5]

Phosphate, whose level is tightly regulated in the human body (physiologic range 0.8-1.5mmol/L), plays vital roles in the regulation of various physiological processes such as membrane integrity, intracellular signaling and skeletal mineralization.[6-8] Hyperphosphatemia accounts for morbidity in 23% of CKD stage 4 patients and about 70% of dialysis patients.[9] Compelling clinical evidence suggests that hyperphosphatemia contributes to higher atherosclerotic death risk in Western CKD patients and the general population.[10-12] Moreover, feeding ApoE-/- mice a phosphate-rich diet resulted in more severe atherosclerotic lesions independently of vascular calcification, while oral phosphate binder could decrease the progression of atherosclerosis in uremic ApoE-/- mice.[13-15] Emerging studies indicate the involvement of hyperphosphatemia in atherogenesis in CKD through disturbed cholesterol homeostasis,[16,17] but the underlying mechanisms remain largely unknown.

Sterol regulatory element-binding protein (SREBP) 2, which is synthesized as an immature precursor embedded in the ER, principally controls the expression of genes involved in cholesterol uptake and biosynthesis. The stability and maturation of precursor SREBP2 relies on binding to SREBP cleavage-activating protein (SCAP), a sterol sensor.[18,19] A small reduction of ER membrane cholesterol alters SCAP conformation, resulting in its detachment from its anchoring protein insulin-induced gene (INSIG) 1 and translocation of SCAP/SREBP2 complex from ER to Golgi, where SREBP2 is enzymatically cleaved and

releases its active NH_2 terminal fragment SREBP2-N. SREBP2-N can enter the nucleus to bind with a sterol regulatory element (SRE) to activate 3-hydroxy-3-methyl-glutaryl coenzyme A reductase (HMGCR) and low-density lipoprotein receptor (LDLr) gene transcription.[20,21] Intracellular cholesterol de-novo synthesis is increased via upregulated HMGCR, and native low-density lipoprotein (LDL) intake is strengthened by upregulated LDLr.

During translocation to the Golgi, asparagine (N)-linked carbohydrates of SCAP are successively modified by α-mannosidase (α-MAN) I, N-acetylglucosamine (GlcNAc) transferase I, and α-MAN II.[22] The modifications cause the N-glycans of SCAP to be heterogeneously converted from a format of high-mannose glycans to complex glycans containing multiple-branches (defined as 'complex-type conversion'). Part of the SCAP protein then recycles back to the ER to form a new complex with another SREBP2, while the remainder is subject to degradation by the ubiquitin proteasome system.[23] Glucose deprivation prohibited N-glycosylation of SCAP, which made it more susceptible to degradation and therefore restricted its bio function in the transactivation of SREBPs.[24] Increased biosynthesis of cholesterol mediated by HMGCR contributes to lipid accumulation and foam cell formation in vascular smooth muscle cells (VSMCs).[25] SCAP dysfunction has been implicated in atherosclerosis observed in chronic inflammatory status and diabetes.[25-29] However, whether increased serum phosphate (P^{3+}) level in CKD patients affects SCAP posttranslational glycosylation, and whether the modifications contribute to the development of ASCVD remains unclear.

In the present study, we analyzed clinical epidemiology data from a Chinese CKD population, which supported our argument that hyperphosphatemia accelerated ASCVD. We also explored the aberrant activation of SCAP-SREBP2 signaling in the arteries of hyperphosphatemic ApoE-/- mice and uremic patients. We sought to determine how

excessive phosphate perturbs SCAP posttranslational glycosylation, causing unregulated intracellular cholesterol synthesis with foam cell formation. These studies provide a novel mechanistic explanation for the accelerated atherosclerosis in CKD population.

Methods

1. A cross-sectional study in Chinese CKD population

A study population including 438 CKD patients from stage 3 to 5 admitted to the First Affiliated Hospital of Chongqing Medical University from January 2013 to February 2016. Serum P^{3+} levels were the mean of three measurements of fasting morning serum P^{3+} concentration within 1 month. All the subjects were categorized into four serum P^{3+} ranges as follows: <1.21mmol/L, 1.22mmol/L~1.46mmol/L, 1.47mmol/L~ 1.78mmol/L and >1.78mmol/L, by quartile spacing strategy. Details were described in supplements. The study was approved by the Human Research Ethics Committee at Chongqing Medical University. All subjects were included after providing informed consent.

2. Study animals

A hyperphosphatemic animal model was established by feeding high phosphate diet (HPD) as previously published.[13] 8 weeks old male ApoE-/- mice were raised with standard chow (n=15) or HPD (n=15) (Baitai Hongda Biotec., Ltd, China) for 16 weeks. The formulas of the main nutrition gradients were shown in Supplemental Table 3. The post valve aortic root (about 5mm in length) was used to prepare frozen serial sections. The remaining aortas were stored in -80°C for mRNA and protein examination. All procedures of the animal study were approved by the Subcommittee on Animal Care Research at Chongqing Medical University.

3. Cell culture

The detailed methods of our primary human aortic VSMCs culture were based on our previous work.[25] The cells of 6^{th} or 7^{th} passages were used for experiments. Phosphate

stocking medium was made of NaH_2PO_4 and Na_2HPO_4 (adjusting pH to 7.40).

4. SCAP protein degradation

The protocols for determining SCAP protein degradation followed previous investigations.[24,26]

5. Crude ER isolation and examination of SCAP N-glycans

Treated VSMCs on four 150cm^2 flasks were harvested to examine the format of SCAP N-glycans following the approach of Nohturfft et al..[22]

6. Microsomes preparation and enzymatic assay of α-MAN II activity

Treated VSMCs on two 150cm^2 flasks were harvested, and the α-MAN II activity was determined using a previously described enzyme-based method and normalized by microsome proteins determined by the Lowry assay.[26]

7. Statistics

Statistical analyses were performed using SPSS 13.0. All data were analyzed by 2-tailed Student's t-test as well as by one-way ANOVA as appropriate. $P < 0.05$ was considered statistically significant.

Results

1. Hyperphosphatemia correlated with increased ASCVD risk in Chinese CKD patients

438 CKD patients were divided into atherosclerosis (AS) and non-atherosclerosis (non-AS) groups according to the diagnosis of ASCVD; their basic characteristics were described in Supplemental Table 1. Hyperphosphatemia and several other parameters such as maintenance dialysis showed positive correlations with the incidence of ASCVD (Supplemental Table 2). Multivariate logistic stepwise regression analysis suggested that serum P^{3+} levels between 1.47mmol/L~1.78mmol/L (P=0.010) and >1.78mmol/L (P=0.002) were positively correlated with the incidence of ASCVD. ASCVD risk increased with rising

serum P^{3+} level (serum P^{3+} level 1.47~1.78mmol/L, OR 2.348; serum P^{3+} level >1.78mmol/L, OR 2.878) (Table 1).

2. Hyperphosphatemia disrupted SCAP mediated cholesterol homeostasis in the atherogenesis of ApoE-/- mice

Four weeks after feeding a HPD, the serum P^{3+} levels of the mice were significantly elevated and sustained until sacrificed (HPD 2.68mmol/L vs standard chow 2.14mmol/L). There were no alterations of other indexes such as total cholesterol (TC) and triglyceride when sacrificed, except for parathyroid hormone, the secondary change of elevated serum P^{3+} levels (Supplemental Table 3). HPD feeding resulted in a more severe atheroma burden relative to standard chow (Figure 1A and 1B). The serum P^{3+} level correlated positively with the atheroma burden in the aortic root (Figure 1C).

We observed transcription changes of cholesterol metabolism-related genes in aortas but not in livers in HPD fed mice (liver data not shown). mRNA levels of HMGCR, LDLr and SREBP2, but not of INSIG1, SCAP, liver X receptor α (LXRα) or ATP-binding cassette transporter A1 (ABCA1), were increased in HPD fed mice (Figure 1D). The protein levels of SCAP, HMGCR and SREBP2-N, but not INSIG1, LDLr, LXRα and ABCA1 were dramatically elevated in HPD fed mice relative to the control (Figure 1E, F). Moreover, immunohistochemistry staining further confirmed SCAP protein increment in the aortas of HPD fed mice (Figure 1G).

3. Excess phosphate induced translocation of SCAP and cholesterol accumulation *in vitro*

VSMCs and macrophages are the main sources of atheromatous foam cells. Neutral lipid deposition was increased when VSMCs and THP-1 macrophages were treated with excess phosphate (3.0mmol/L) (Figure 2A and Supplemental Figure 1A). The TC and cholesterol ester (CE) levels, but not free cholesterol (FC) in excess phosphate-treated VSMCs were

significantly higher than in controls (Figure 2B). Excess phosphate increased intracellular TC but not CE or FC in THP-1 macrophages (Supplemental Figure 1B).

Excess phosphate increased the mRNA levels of HMGCR, LDLr and SREBP2, but not INSIG1, LXRα or ABCA1 (Figure 2C and Supplemental Figure 1C). It did not affect the protein levels of INSIG1, LDLr, LXRα and ABCA1, but increased that of HMGCR and SREBP2-N (Figure 2D, E and Supplemental Figure 1D, E). Excess phosphate did not affect SCAP mRNA expression (Figure 2H and Supplemental Figure 1H) but increased its protein level (Figure 2F, G and Supplemental Figure 1F, G). Excess phosphate enhanced co-localization of SCAP within the Golgi (Figure 2I and Supplemental Figure 1I). VSMCs were more sensitive to excess phosphate than THP-1 macrophages so were used alone in subsequent experiments. Levels of LDLr mRNA increased 1.35-fold in excess phosphate treated VSMCs, but its protein expression reached only 1.16-fold of control. This small variation in LDLr protein level did not increase Dil-LDL uptake as shown by fluorescence photography (Figure 2J) and fluorospectrophotometry (Figure 2K). In line with our *in vivo* findings we found that excess phosphate increased SCAP protein at the post-transcriptional stage, enhancing SCAP escort for SREBP2 transactivation to upregulate the expression of HMGCR, thus facilitating cholesterol de-novo synthesis and intracellular cholesterol accumulation.

4. Excess phosphate promoted intracellular cholesterol accumulation via SCAP-SREBP2-HMGCR pathway in VSMCs

The mRNA levels of HMGCR and SREBP2 were stably increased when the concentration of phosphate rose from 1.0 to 5.0mmol/L without affecting SCAP mRNA levels (Supplemental Figure 2A). HMGCR and SCAP protein increased as the phosphate concentration elevated (Supplemental Figure 2B), suggesting a dose-dependent SCAP response to phosphate signaling. A physiological phosphate concentration (1.0mmol/L)

changed neither SCAP nor HMGCR protein levels over 72-hour time course but excess phosphate increased HMGCR and SCAP protein levels dramatically and they remained high after 24 hours (Supplemental Figure 2C).

Sodium-dependent phosphate cotransporter (NPC) is the main channel for phosphate uptake in VSMCs, to which phosphoformate sodium (PFA) is a specific competitive inhibitor that can dose-dependently block NPC.[30] PFA did not reduce HMGCR and SREBP2 mRNA levels with a physiological concentration of phosphate, but inhibited their excess phosphate elevated expressions (Figure 3A, B). PFA did not affect SCAP mRNA levels (Figure 3A), but overrode the increased SCAP, HMGCR and SREBP2-N protein levels observed after excess phosphate treatment (Figure 3B). Meanwhile, PFA inhibited intracellular TC and CE accumulation induced by excess phosphate, but did not change their levels within the physiological concentration of phosphate (Figure 3C). These results imply that blocking VSMC phosphate uptake can abrogate the activation of SCAP signaling by excess phosphate.

When knocking down SCAP by shRNA, the mRNA and protein levels of HMGCR and SCAP decreased, even in the presence of excess phosphate, which also reduced SREBP2 mRNA level and SREBP2-N in the nucleus (Figure 3D and 3E). Meanwhile, knocking down SCAP reduced intracellular TC and CE contents (Figure 3F). Knocking down SREBP2 led to much-reduced mRNA levels of HMGCR and SREBP2 but not of SCAP, even in the presence of excess phosphate (Figure 3G). Excess phosphate increased SCAP protein level, but knocking down SREBP2 decreased HMGCR and SREBP2-N in the nucleus (Figure 3H). Moreover, knocking down SREBP2 reduced intracellular TC and CE content and offset the accumulating effects on them of excess phosphate (Figure 3I). These results indicated that excess phosphate specifically promoted cholesterol accumulation in VSMCs via SCAP-SREBP2-HMGCR signaling.

5. Excess phosphate delayed SCAP degradation by promoting complex-type

conversion of its N-glycans

Cycloheximide (CHX) is an inhibitor for intracellular protein synthesis, which can be used to determine the half-life of proteins in molecular biology.[24,26] SCAP protein levels significantly decreased at the 8th hour after CHX treatment and reduced to 22% at the 24th hour compared to that of hour 0 within a physiological phosphate concentration. However, with excess phosphate, the SCAP protein at the 24th hour remained at 48.9% of that at hour 0 (Figure 4A and B), indicating that excess phosphate increased SCAP protein retention by delaying its degradation. GlcNAc (20mmol/L), which facilitates N-glycosylation, significantly increased mRNA levels of HMGCR and SREBP2, while tunicamycin (Tuni, 1μg/ml, an inhibitor of N-glycosylation) decreased them even in the presence of excess phosphate (Figure 4C). Neither GlcNAc nor Tuni altered mRNA level of SCAP (Figure 4D). However, GlcNAc increased SCAP, HMGCR and SREBP2-N protein levels equivalent to those of excess phosphate, and Tuni decreased them in the same condition (Figure 4E). These data implied that the effects of excess phosphate on SCAP signaling were probably mediated by altering the N-glycans of SCAP.

SCAP contains a glycosylated peptide of 170 aa that is protected from proteolysis by trypsin.[31] This trypsin protected fragment acquires two N-linked high-mannose-type glycans which are sensitive to hydrolysis by endoglycosidase H (endo. H) when the nascent SCAP was synthesized. The two glycans will become endo. H resistant when further modified by a-MAN II in the Golgi, converting to the complex-type glycans.[22] Within the physiological phosphate concentration, N-glycans of SCAP largely remained high-mannose-type, as shown that the apparent mass of the most trypsin protected fragments became smaller (without glycans) after endo-H digestion which hydrolyzed their high-mannose-type glycans (Figure 4F, lane 1). Excess phosphate converted >90% of SCAP N-glycans to the complex-type, because most trypsin protected fragments are still with glycans after endo. H digestion (endo.

H resistant) (Figure 4F, lane 4 vs lane 1). Excess phosphate was more efficient than GlcNAc in facilitating the complex-type conversion of SCAP N-glycans (Figure 4F, lane 4 vs lane 2). Tuni nearly abolished phosphate-induced conversion of SCAP N-glycans from high-mannose-type to the complex-type, as shown by half of the trypsin protected fragments remaining sensitive to endo. H (Figure 4F, lane 5 vs lane 4), which hydrolyzed them to make the apparent mass of the fragments as small as if N-glycans had been removed, whether or not they have been modified in the Golgi, using endoglycosidase PNGase F (as a positive control) (Figure 4F, lane 6). Interestingly, we found that both GlcNAc and excess phosphate increased SCAP colocalization with Golgi apparatus (Figure 4G GlcNAc and Pi vs ctrl), which was attenuated by Tuni (Figure 4G Tuni vs ctrl), even in the presence of excess phosphate (Figure 4G Tuni vs Pi+Tuni).

6. Excess phosphate enhanced the activity of α-MAN 2A1 and 2A2 *in vitro*

With the increase of phosphate concentrations, α-MAN II activity increased (Figure 5A). Interestingly, PFA did not affect α-MAN II activity within physiological phosphate concentrations but could reverse the elevated enzyme activity by excess phosphate (Figure 5B). Swainsonine (Swain) is a potent and selective inhibitor of α-MAN II. Excess phosphate significantly increased the activity of α-MAN II, which can be inhibited by Swain (2.5μg/mL) (Figure 5C). This inhibition also reduced TC and CE levels, even in the presence of excess phosphate (Figure 5D).

α-MAN 2A1 and 2A2 are the two isoforms of α-MAN II, which are located mainly in the Golgi and manipulate complex-type conversion of SCAP N-glycans.[32,33] Excess phosphate did not affect both the gene (Figure 5E) and protein (Figure 5F) levels of α-MAN 2A1 and 2A2. However, knocking down either α-MAN 2A1 or α-MAN 2A2 with shRNA suppressed both HMGCR and SREBP2 mRNA expression, which can be reversed by excess phosphate (Figure 5G). In the same manner, knocking down either α-MAN 2A1 or α-MAN

2A2 with a shRNA significantly decreased α-MAN II activity, and the effects can be alleviated by excess phosphate (Figure 5H). Knocking down the two isoforms simultaneously with both shRNA resulted in accelerated SCAP degradation after CHX treatment, and this effect can be disrupted by excess phosphate (Figure 5I and J). Knocking down the two isoforms simultaneously also reduced SCAP colocalization with Golgi, which was reversed by excess phosphate (Figure 5K).

7. Hyperphosphatemia enhanced the activity of arterial α-MAN II

Hyperphosphatemia did not affect the levels of the genes (Figure 6A) and proteins (Figure 6B) of α-MAN 2A1 and 2A2, but significantly increased α-MAN II activity in the aorta of ApoE-/- mice (Figure 6C). We also detected elevated SCAP protein levels in radial arteries of uremic patients with hyperphosphatemia (with serum phosphate level of 2.43±0.57mmol/L) by immunohistochemistry staining (Figure 6D). There was increased activity of α-MAN II, when compared with the control group (with serum phosphate level of 1.27±0.15mmol/L) (Figure 6E).

Discussion

In this study, we report for the first time that hyperphosphatemia in Chinese CKD patients is an independent risk factor for ASCVD, and that higher serum P^{3+} levels are significantly associated with a higher ASCVD risk, which accords with clinical observations in Western countries.[10-12] Our present work using a mouse model also revealed evidence that the severity of the aortic atheroma burden paralleled serum P^{3+} levels. These results demonstrated a clear link between hyperphosphatemia and ASCVD.

The known mechanisms involved in the pathophysiology of phosphate-induced cardiovascular risk are vascular calcification and endothelial dysfunction,[7,8,34] but the potential link between hyperphosphatemia and atherosclerosis is reportedly uncertain.[14] Previous studies by Phan and Ellam both showed that hyperphosphatemia accelerates

atherogenesis in ApoE -/- mice, but the molecular mechanisms remain unclear.[13-14] Our data obtained in the present study confirmed the pro-atherosclerotic effect of hyperphosphatemia and showed for the first time that phosphate has a direct pro-atherogenic role by perturbing VSMC local cholesterol metabolism. We did not detect significant changes in blood lipid levels in our hyperphosphatemic mouse model, but aortic atheroma lesions increased significantly. In line with this observation, the lipid profile was not affected by a HPD in the study from Ellam, and sevelamer benefited atherogenesis in uremic ApoE-/- mice with hyperphosphatemia without impacting circulating cholesterol as in the study from Phan.[14,15] These studies suggest that atherosclerosis induced by hyperphosphatemia is not necessarily dependent on hyperlipidemia and that disturbed cholesterol homeostasis (for example increased intracellular cholesterol synthesis) of local cells on the vessel wall could lead to an accumulation of cholesterol in the arteries. In fact, local vascular lipid homeostasis could be affected by phosphate or other factors (for example inflammation) without changes of overall lipid profiles.[25,28] We and others have demonstrated a weak association between LDL cholesterol level and coronary risk in CKD.[2,35].

Modified LDL uptake via CD 36 and scavenger receptor A (SRA) was thought to be the main pathway for atherogenic cholesterol accumulation in artery cells.[36] However, intracellular cholesterol homeostasis is coordinately regulated by cholesterol influx, efflux and de-novo synthesis. Emerging evidence has highlighted the importance of HMGCR mediated cholesterol biosynthesis in atherogenesis.[25,37,38] Excess phosphate significantly increased both mRNA and protein expression of HMGCR in VSMCs and macrophages. The elevation of HMGCR level was proven to directly lead to its increased activity for catalyzing acetyl-CoA into mevalonic acid, the rate-limiting step in cholesterol de-novo synthesis and exacerbating cholesterol accumulation.[24] Meanwhile, excess phosphate neither increased LDL uptake via LDLr nor affected LXRα and ABCA1 expression which mediates cholesterol

efflux from cells. Therefore, the cholesterol accumulation observed in this study was mainly because of increased de-novo cholesterol synthesis by HMGCR.

By generating the heterozygote SM22α-Cre:SCAP$^{flox/+}$: ApoE$^{-/-}$mice, we have previously reported the importance of SCAP in atherosclerotic foam cell formation in *vivo*.[27] Here, blocking phosphate transport by PFA and gene silencing of SCAP or SREBP2 dramatically interrupted the effect of excess phosphate on SCAP/SREBP2 signaling and cholesterol accumulation, indicating that SCAP may act as a key phosphate-responsive protein, which orchestrates cholesterol homeostasis by controlling SREBP2 activation.

The biosynthesis of N-glycans begins when nascent SCAP is translocated into the lumen of the ER.[22,39] Before SCAP transits to the Golgi, its glycan structure is cleaved by α-MAN I in the ER.[22,39] These high-mannose-type glycans are sensitive to endo. H digestion.[40] The glycans can then be catalyzed by GlcNAc transferase I in the medial Golgi, which allows for the generation of glycan branches. Successively, the glycans are converted to multi-branched, complex-type glycans by decorations of sialic acid, galactose, and fucose in the trans-Golgi, which is catalyzed by α-MAN II (2A1 and 2A2). They then became resistant to endo. H,[22,41] suggesting that α-MAN II is the key enzyme for the formation of SCAP complex-type glycans.

Excess phosphate raised the activity of α-MAN II, leading to the conversion of most SCAP glycans from the high-mannose-type to the complex-type (Figure 4F lane 4). Gene silencing of α-MAN 2A1 and 2A2 blocked this conversion, which further differentiated the detrimental role of α-MAN II in raised phosphate conditions, indicating that α-MAN 2A1 and 2A2 controlled complex-type conversion of SCAP N-glycans could be key factors for the pathogenesis of foam cell formation. Our findings further revealed that SCAP with complex-type glycans is more resistant to degradation than SCAP with high-mannose-type glycans (combining the results from Figure 4A/B and Figure 4F). A previous study

demonstrated in glioblastoma cells preventing N-glycosylation by glucose depletion, accelerated the proteasome-dependent degradation of SCAP.[24] Our study suggested that not only N-glycosylation but the complex-type conversion of N-glycans by the α-MAN II could be decisive for the stability of SCAP. The best model to test the specific role of phosphate on lipid homeostasis is SCAP VSMCs knockout mice. However, SCAP is an essential molecule for the survival of eukaryotes. Both global and VSMC-specific SCAP KO are lethal for mice. This is one limitation of this study.

Overall, our study demonstrated that excess phosphate enters VSMCs via NPC and promotes the complex-type conversion of SCAP N-glycans by augmenting the activity of α-MAN II, which increases SCAP half-life and protein levels. As a result, SCAP with complex-type glycans recycle around the ER and Golgi and over-activate SREBP2, leading to robust cholesterol de-novo synthesis and therefore intracellular cholesterol accumulation and foam cell formation (Figure 7). We provide a new view of a link between hyperphosphatemia and lipid metabolic disturbance, both of which are important risk factors for atherosclerosis. These findings may help understanding of the pathogenesis of accelerated atherosclerosis and the high incidence of ASCVD in patients with CKD. It may also contribute to the design of effective dual therapeutic strategies targeting both phosphate and lipid metabolisms in the CKD population.

Author contributions: C.Z., N.O.Y., X.Z.R. and Q.H. contributed to the design of the study. C.Z., N.O.Y., T.T.Z., and Q.L. conducted the experiments. H.G., T.T.Z. and N.O.Y. collected the clinical data. C.Z., T.T.Z. and N.O.Y. analyzed data. C.Z., X.Z.R., J.F.M. and Z.V. wrote the manuscript.

Competing interests: None.

Supplementary Material

1 Supplemental Figure 1

2 Supplemental Figure 2

3 Supplemental Table 1

4 Supplemental Table 2

5 Supplemental Table 3

6 Supplemental Table 4

7 Supplemental Table 5

8 Supplemental Table 6

Supplementary information is available on Kidney International's website.

Figure legends

Figure 1. Hyperphosphatemia promoted atherosclerosis and disrupted SCAP mediated cholesterol homeostasis in the aorta of ApoE-/- mice. (A)-(B) The hyperphosphatemia model was established by feeding ApoE-/- mice with HPD, whose littermates receiving normal chow served as control. The longitudinal dissection of the aortic tissue or aortic root frozen serial sections of the mice were prepared and stained by ORO method when they were sacrificed. (A) Representative images of atheroma lesions on the longitudinal dissection of aorta, photographed by a camera (Canon, Japan) (n=6 mice per group). (B) Representative images of atheroma lesions on the aortic root sections of mice, observed under microscopy (Scale bar= 100μm); quantification of the atheroma burden was processed on six sections of each aorta by Image J software, each section was from every ten successive sections of one mouse. The results were means ±SD of plaque area/ aorta area (%) (n=7 mice per group). (C) The correlation between atheroma burden and serum phosphate level, analyzed by linear

regression analysis (n=14 mice). (D) The mRNA expression of the cholesterol metabolic components analyzed by Real-time PCR; β-actin served as the reference gene. Values are means ±SD from 7 mice of each group. (E) The protein levels of the cholesterol metabolic components examined by Western blotting; the demonstrated bands were typical from 3 experimental repeats. β-actin served as the domestic control for the cytoplasmic protein, and lamin A served as the reference for the nuclear protein. (F) The densitometric scans of protein bands represented by means ±SD, normalized by comparison with reference protein and expressed as a percentage of control (n=6 mice per group). (G) Representative photomicrographs of SCAP antibody-stained immunohistochemistry (ICH) sections from the mice aortic root (Scale bar=100μm) (n=6 mice per group). Statistical significance was assessed using 2-tailed Student' s t-test in B, D and F. * P<0.01, ** P<0.05.

Figure 2. Excess phosphate induced translocation of SCAP and cholesterol accumulation in VSMCs. (A)-(I). The VSMCs were cultured in experimental medium with or without excess phosphate for 24 hours. (A) The intracellular neutral lipids stained by ORO. The results are typical of those observed in four separate experiments. Scale bar=50μm. (B) Quantification of intracellular FC and CE. Values are means ±SD from 3 experimental repeats (n=12 per group). (C and H) The gene expressions of the cholesterol metabolic components determined by Real-time PCR. β-Actin served as the reference gene. Values are means ±SD from 3 experimental repeats (n=9 per group). (D and F) The protein levels of the cholesterol metabolic components examined by Western blotting. The demonstrated bands were typical from 3 experimental repeats. β-Actin served as the domestic control for the

cytoplasmic protein, and lamin A served as the reference for the nuclear protein. (E and G) The densitometric scans of protein bands represented by means ±SD from 3 experimental repeats (n=6 per group), normalized by comparison with reference protein and expressed as a percentage of control. (I) The colocalization of SCAP with Golgi apparatus observed by confocal microscopy (as arrow pointed). The results are typical of those observed in four separate experiments. Scale bar=50μm. (J)-(K). The VSMCs were incubated with Dil-LDL (25μmol/L) for 4 hours. (J) Cells were fixed with 4% paraformaldehyde and captured by fluorescence microscopy; the red fluorescence represents Dil-LDL uptake via LDLr. Scale bar=100μm. (K) Cells protein were prepared with lysis buffer, Dil-LDL fluorescence intensity were quantified by fluorescence spectrophotometer. The histogram represents means ±SD of Dil-LDL fluorescence intensity from 3 experimental repeats (n=12 per group), normalized by total protein volume. Statistical significance was assessed using 2-tailed Student' s t-test in B, C, E, G, H and K. *P<0.01, **P<0.05. Pi, excess phosphate.

Figure 3. Excess phosphate promoted intracellular cholesterol accumulation via SCAP-SREBP2-HMGCR pathway in VSMCs. The VSMCs were cultured in experimental medium with or without excess phosphate and indicated treatments for 24 hours. (A, D and G) The gene expression determined by Real-time PCR. β-Actin served as the reference gene. Values are means ±SD from 3 experimental repeats (n=12). (B, E and H) The protein levels examined by Western blotting. The demonstrated bands were typical from 3 experimental repeats, β-actin served as the reference for cytoplasmic proteins, lamin A served as the reference for proteins in the nucleus. (C, F and I) Quantification of intracellular FC and CE. Values are mean ±SD of duplicate wells from 3 experimental repeats (n=12). Statistical significance was assessed using one-way ANOVA with Bonferroni or Tamhane'sT2 as

appropriate in A, D, F, G, I, J, and L. * P<0.01. Pi, excess phosphate.

Figure 4. Excess phosphate delayed SCAP degradation by promoting complex-type conversion of its N-glycans. (A)-(B) The VSMCs were cultured in experimental medium with 50μmol/L CHX in the absence or presence of excess phosphate for the indicated times. (A) The protein levels examined by Western blotting. The demonstrated bands were typical from 3 experimental repeats. (B) The densitometric scans of protein bands by the Image-J software. Values are means ±SD from 3 experiments (n=6). (C)-(G) The VSMCs were cultured in experimental medium with or without excess phosphate and indicated treatments for 24 hours. (C and D) The gene expression determined by Real-time PCR. β-actin served as the reference gene. Values are means ±SD from 3 experiments (n=12). (E) The protein levels examined by Western blotting. The demonstrated bands were typical from 3 experimental repeats. Lamin A served as the reference for proteins in the nucleus. β-actin served as the reference for cytoplasmic proteins. (F) N-glycans of SCAP was analyzed as we described in the Materials and methods section. (G) The colocalization of SCAP with Golgi apparatus observed by confocal microscopy (as arrow pointed). The results are typical of those observed in four separate experiments. Scale bar=50μm. Statistical significance was assessed using one-way ANOVA with Bonferroni or Tamhane'sT2 as appropriate in B, C and D. * P<0.01; ** P<0.05. Pi, excess phosphate.

Figure 5. Excess phosphate enhanced the activity of α-MAN 2A1 and 2A2 *in vitro*. (A)-(H) and (K) The VSMCs were cultured in experimental medium with or without excess phosphate and indicated treatments for 24 hours. (A, B, C and H) The activity of α-MAN II determined by the enzymatic assay as we described in the Materials and methods section. Values are means ±SD of duplicate wells from 3 experiments (n=9). (D) Intracellular FC and CE assayed by a quantitative method. Values are mean ±SD of duplicate wells from 3

experiments (n=12). (E and G) The gene expression determined by Real-time PCR. β-Actin served as the reference gene. Values are means ±SD of duplicate wells from 3 experiments (n=12). (F) The protein levels examined by Western blotting. The demonstrated bands were typical from 3 experimental repeats. β-Actin served as the reference for cytoplasmic proteins. (K) The colocalization of SCAP with Golgi apparatus observed by confocal microscopy (as arrow pointed). The results are typical of those observed in four separate experiments. Scale bar=50μm. (I)-(J) The VSMCs were cultured in experimental medium with 50μmol/L CHX in the absence or presence of excess phosphate and transfection of both shRNA for α-MAN 2A1 and 2A2 for 16 hours. (I) The SCAP protein levels examined by Western blotting. The demonstrated bands were typical from 3 experimental repeats. (J) The densitometric scans of SCAP protein bands by the Image-J software. Values are means ±SD of duplicate wells from 3 experiments (n=6). Statistical significance was assessed using one-way ANOVA with Bonferroni or Tamhane'sT2 as appropriate in A, B, C, D, G, H and J, and 2-tailed Student's t test in E. * $P<0.01$. ** $P<0.05$. Pi, excess phosphate.

Figure 6. Hyperphosphatemia enhanced the activity of α-MAN II in the artery. (A) The mRNA was extracted from the aorta tissue of the hyperphosphatemia mice and control. The gene expression was analyzed by Real-time PCR method. β-actin served as the reference gene. Values are means ±SD from 7 mice of each group. (B) The protein was extracted from the aorta, and the protein levels were examined by Western blotting. The demonstrated bands were typical from 3 experimental repeats (n=6 mice). β-actin served as the loading control. (C) The activity of α-MAN II in the aorta tissue of ApoE-/- mice. Values are means ±SD from 7 mice of each group. (D) Representative photomicrographs of SCAP antibody-stained Immunohistochemistry (ICH) sections from the radial artery of uremic patients (Scale bar= 100μm). The values of semiquantitative analysis for the positive areas are expressed as the

means ±SD from 8 patients at each group. (E) The activity of α-MAN II in the radial artery of uremia patients. Values are means ±SD from 8-9 patients of each group. Statistical significance was assessed using 2-tailed Student's t-test in A, C and E. * P<0.01.

Figure 7. Schematic diagram: Enhanced complex-type conversion of SCAP N-glycans by hyperphosphatemia via aberrant activation of α-MAN II leading to robust cholesterol synthesis and atherogenesis. (A) Excess phosphate enters VSMC via NPC and enhances complex-type conversion of SCAP N-glycans by augmenting the activity of α-MAN II. As a result, the degradation of SCAP with complex glycans slows down, which recycles around ER and Golgi and overactivates SREBP2, leading to robust cholesterol de-novo synthesis, and thereby intracellular cholesterol accumulation and foam cell formation. Pi, phosphorus. NPC, Na-Pi cotransporter. α-MAN II, α-mannosidase II. (B) Signaling cascade for excess phosphate uptake to complex-type conversion of SCAP N-glycans and robust cholesterol de-novo synthesis.

References

1. GBD Chronic Kidney Disease Collaboration. Global, regional, and national burden of chronic kidney disease, 1990–2017: a systematic analysis for the Global Burden of Disease Study 2017. Lancet. 2020; 395:709-733

2. Reiss AB, Voloshyna I, De Leon J, et al. Cholesterol Metabolism in CKD. Am J Kidney Dis. 2015; 66:1071-1082.

3. Wanner C, Krane V, März W, et al. German Diabetes and Dialysis Study Investigators, Atorvastatin in patients with type 2 diabetes mellitus undergoing hemodialysis. N Engl J Med. 2005; 353:238-248.

4. Fellström BC, Jardine AG, Schmieder RE, et al. Rosuvastatin and cardiovascular events in patients undergoing hemodialysis. N Engl J Med. 2009; 360:1395-1407.

5. Baigent C, Landray MJ, Reith C, et al. The effects of lowering LDL cholesterol with simvastatin plus ezetimibe in patients with chronic kidney disease (Study of Heart and Renal Protection): a randomised placebo-controlled trial. Lancet. 2011; 377:2181-2192.

6. Michigami T, Kawai M, Yamazaki M, et al. Phosphate as a Signaling Molecule and Its Sensing Mechanism. Physiol Rev. 2018; 98:2317-2348.

7. Vervloet MG, Sezer S, Massy ZA, et al. The role of phosphate in kidney disease. Nat Rev Nephrol. 2017; 13:27-38.

8. Yamada S, Giachelli CM. Vascular calcification in CKD-MBD: Roles for phosphate, FGF23, and Klotho. Bone. 2017; 100:87-93.

9. Vervloet MG, van Ballegooijen AJ. Prevention and treatment of hyperphosphatemia in chronic kidney disease. Kidney Int. 2018; 93:1060-1072.

10. Foley RN, Collins AJ, Herzog CA, et al. Serum phosphorus levels associate with coronary atherosclerosis in young adults. J Am Soc Nephrol. 2009; 20:397-404.

11. Dhingra R, Sullivan LM, Fox CS, et al. Relations of serum phosphorus and calcium

levels to the incidence of cardiovascular disease in the community. Arch Intern Med. 2007; 167:879-855.

12. Narang R, Ridout D, Nonis C, et al. Serum calcium, phosphorus and albumin levels in relation to the angiographic severity of coronary artery disease. Int J Cardiol. 1997; 60:73-79.

13. Ellam T, Wilkie M, Chamberlain J, et al. Dietary phosphate modulates atherogenesis and insulin resistance in apolipoprotein E knockout mice-brief report. Arterioscler Thromb Vasc Biol. 2011; 31:1988-1990.

14. Phan O, Ivanovski O, Nguyen-Khoa T, et al. Sevelamer prevents uremia-enhanced atherosclerosis progression in apolipoprotein E-deficient mice. Circulation. 2005; 112:2875-2882.

15. Igor G Nikolov, Nobuhiko Joki, Thao Nguyen-Khoa, et al. Lanthanum carbonate, like sevelamer-HCL, retards the progression of vascular calcification and atherosclerosis in uremic apolipoprotein E-deficient mice. Nephrol Dial Transplant. 2012; 27:505-513.

16. Ellam TJ, Chico TJ. Phosphate: The new cholesterol? The role of the phosphate axis in non-uremic vascular disease. Atherosclerosis. 2012; 220:310-318.

17. Tanaka S, Yamamoto H, Nakahashi O, et al. Dietary phosphate restriction induces hepatic lipid accumulation through dysregulation of cholesterol metabolism in mice. Nutr Res. 2013; 33:586-593.

18. Shao W, Espenshade PJ. Expanding roles for SREBP in metabolism. Cell Metab. 2012; 16:414–419.

19. Kuan YC, Takahashi Y, Maruyama T, et al. Ring finger protein 5 activates sterol regulatory element-binding protein 2 (SREBP2) to promote cholesterol biosynthesis via ubiquitinating SREBP chaperone SCAP. J Biol Chem. 2020; pii: jbc.RA119.011849.

20. Michael S. Brown, Arun Radhakrishnan, et al. Retrospective on Cholesterol Homeostasis: The Central Role of Scap. Annu Rev Biochem. 2018; 87:783-807.

21. Gao Y, Zhou Y, Goldstein JL, et al. Cholesterol-induced conformational changes in the sterol-sensing domain of the Scap protein suggest feedback mechanism to control cholesterol synthesis. J Biol Chem. 2017; 292:8729-8737.

22. Nohturfft A, DeBose-Boyd RA, Scheek S, et al. Sterols regulate cycling of SREBP cleavage-activating protein (SCAP) between endoplasmic reticulum and Golgi. Proc Natl Acad Sci U S A. 1999; 96:11235-11240.

23. Shao W, Espenshade PJ. Sterol regulatory element-binding protein (SREBP) cleavage regulates Golgi-to-endoplasmic reticulum recycling of SREBP cleavage-activating protein (SCAP). J Biol Chem. 2014; 289:7547-7557.

24. Cheng C, Ru P, Geng F, et al. Glucose-mediated N-glycosylation of SCAP Is Essential for SREBP-1 Activation and Tumor Growth. Cancer Cell. 2015; 28:569-581.

25. Chen Y, Ku H, Zhao L, et al. Inflammatory stress induces statin resistance by disrupting 3-hydroxy-3-methylglutaryl-CoA reductase feedback regulation. Arterioscler Thromb Vasc Biol. 2014; 34:365-376.

26. Yuan Y, Zhao L, Chen Y, et al. Advanced glycation end products (AGEs) increase human mesangial foam cell formation by increasing Golgi SCAP glycosylation in vitro. Am J Physiol Renal Physiol. 2011; 301: F236-243.

27. Li D, Chen A, Lan T, et al. SCAP knockdown in vascular smooth muscle cells alleviates atherosclerosis plaque formation via up-regulating autophagy in ApoE-/- mice. FASEB J. 2019; 33:3437-3450.

28. Ruan XZ, Varghese Z, Powis SH, et al. Dysregulation of LDL receptor under the influence of inflammatory cytokines: A new pathway for foam cell formation. Kidney Int. 2001; 60:1716-1725.

29. Ma KL, Ruan XZ, Powis SH, et al. Inflammatory stress exacerbates lipid accumulation in hepatic cells and fatty livers of apolipoprotein E knockout mice. Hepatology. 2008;

48:770-781.

30. Jono S, McKee MD, Murry CE, et al. Phosphate regulation of vascular smooth muscle cell calcification. Circ Res. 2000; 87: E10-17.

31. Nohturfft A, Brown MS, Goldstein JL. Topology of SREBP cleavage-activating protein, a polytopic membrane protein with a sterol-sensing domain. J Biol Chem. 1998; 273:17243-17250.

32. Daniel PF, Winchester B, Warren CD. Mammalian alpha-mannosidases--multiple forms but a common purpose? Glycobiology. 1994; 4:551-566.

33. Moremen KW. Golgi alpha-mannosidase II deficiency in vertebrate systems: implications for asparagine-linked oligosaccharide processing in mammals. Biochim Biophys Acta. 2002; 1573:225-235.

34. Di Marco GS, König M, Stock C, et al. High phosphate directly affects endothelial function by downregulating annexin II. Kidney Int. 2013; 83:213-222.

35. Xiong Z Ruan, Zac Varghese, John F Moorhead. An update on the lipid nephrotoxicity hypothesis. Nat Rev Nephrol. 2009; 5:713-721.

36. Smirnov AN. Lipid signaling in the atherogenesis context. Biochemistry (Mosc). 2010; 75:793-810.

37. Sakai K, Nagashima S, Wakabayashi T, et al. Myeloid HMG-CoA (3-Hydroxy-3-Methylglutaryl-Coenzyme A) Reductase Determines Atherosclerosis by Modulating Migration of Macrophages. Arterioscler Thromb Vasc Biol. 2018; 38:2590-2600.

38. Hwang S, Hartman IZ, Calhoun LN, et al. Contribution of Accelerated Degradation to Feedback Regulation of 3-Hydroxy-3-methylglutaryl Coenzyme A Reductase and Cholesterol Metabolism in the Liver. J Biol Chem. 2016; 291:13479-13494.

39. Zhang X, Wang Y. Glycosylation Quality Control by the Golgi Structure. J Mol Biol. 2016; 428:3183-3193.

40. Kornfeld R, Kornfeld S. Assembly of asparagine-linked oligosaccharides. Annu Rev Biochem. 1985; 54:631-664.

41. Moremen KW, Tiemeyer M, Nairn AV. Vertebrate protein glycosylation: diversity, synthesis and function. Nat Rev Mol Cell Biol. 2012; 13:448-462.

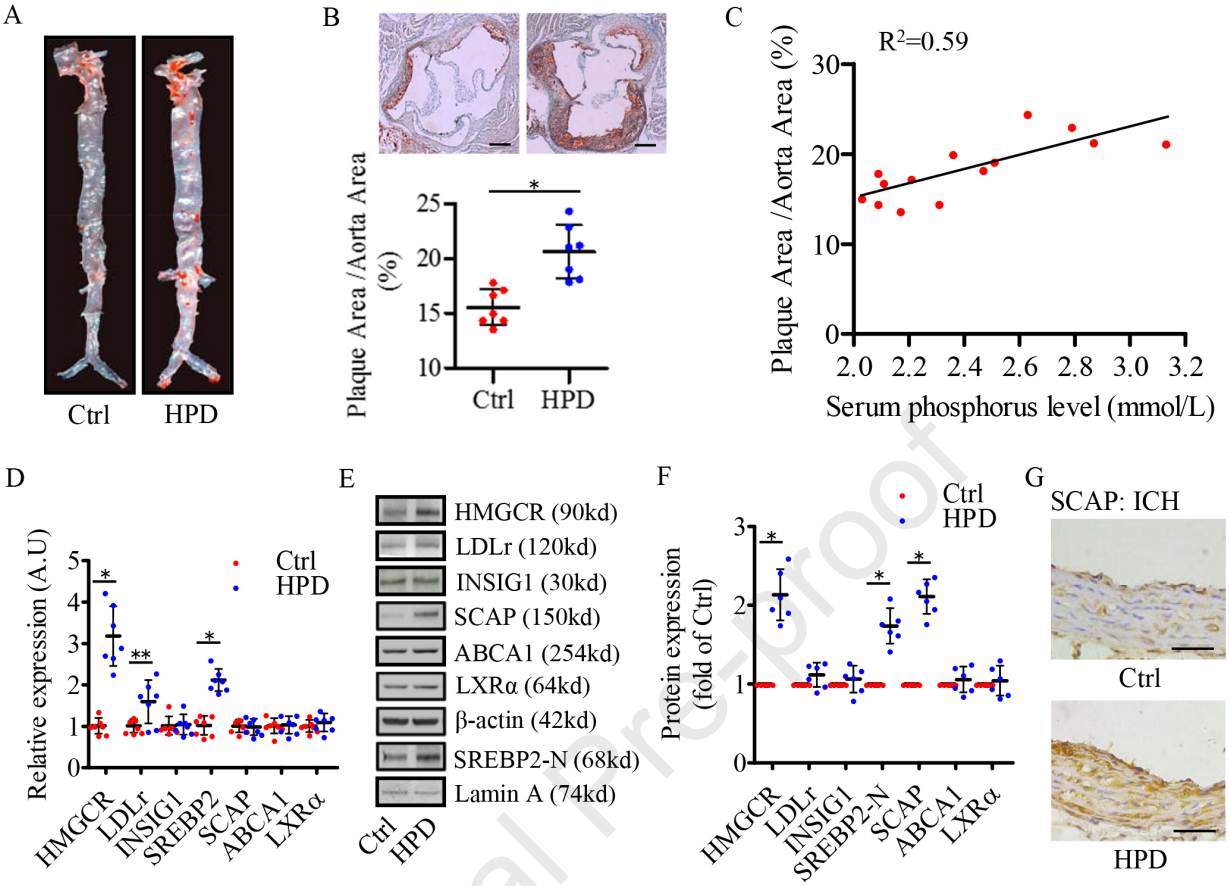

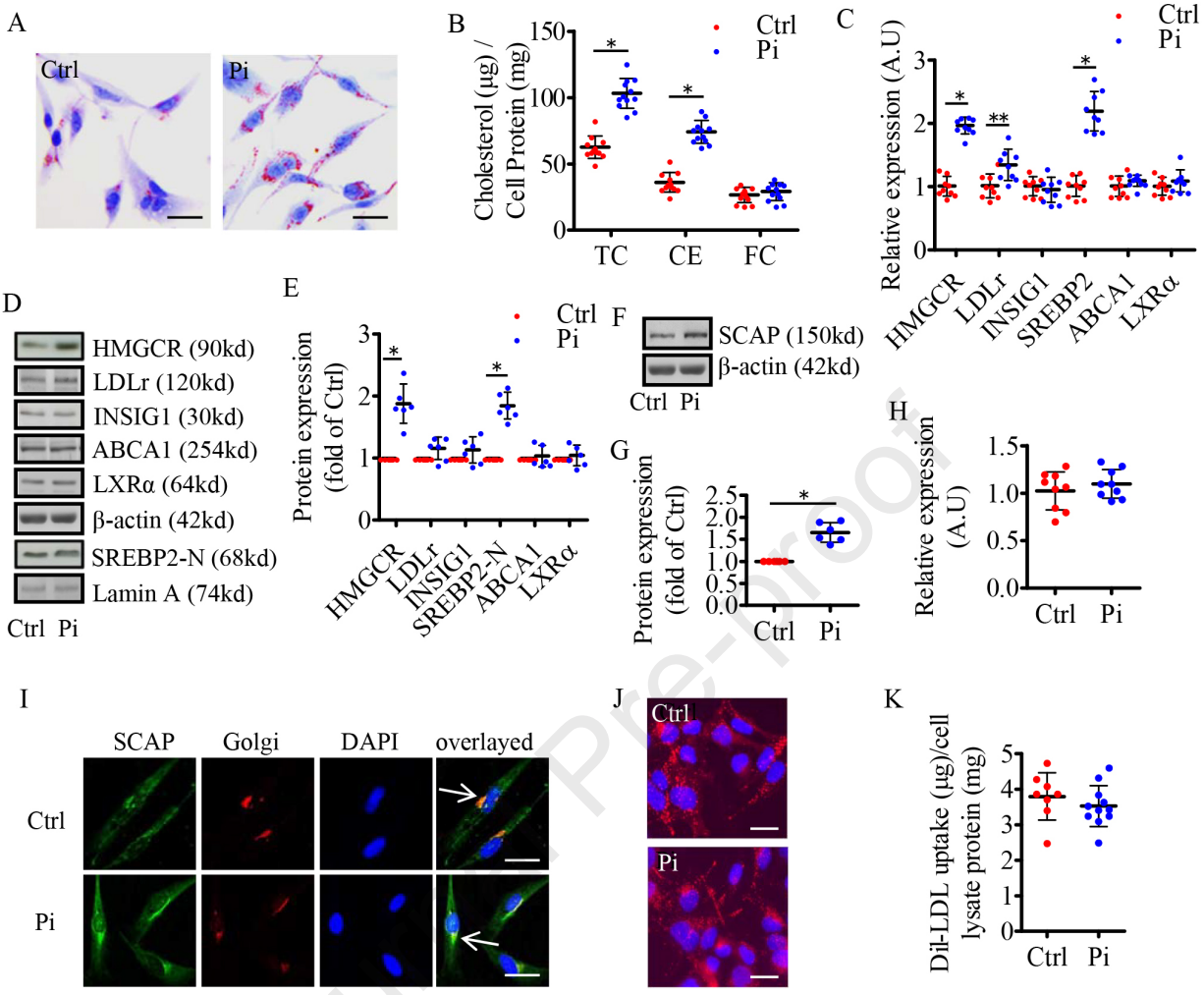

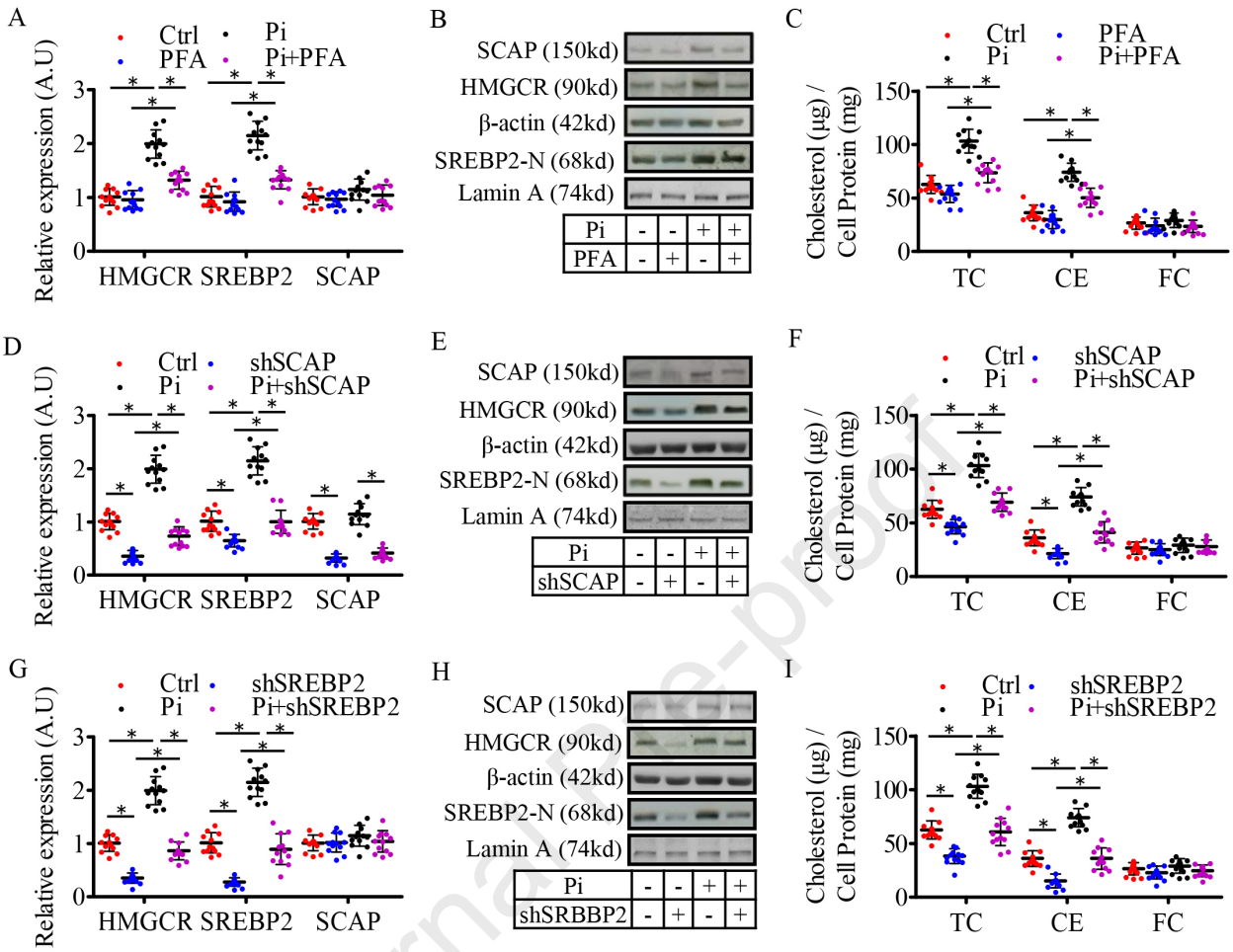

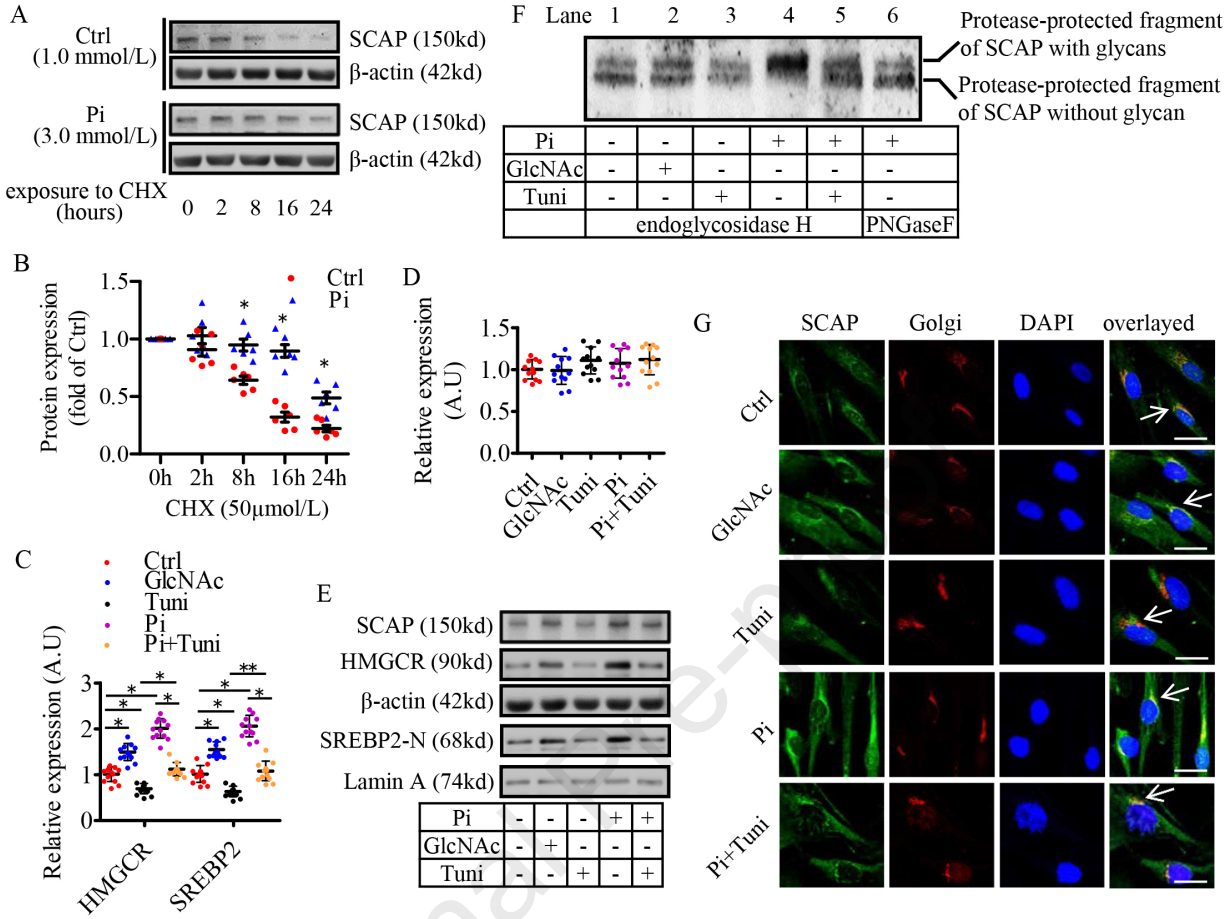

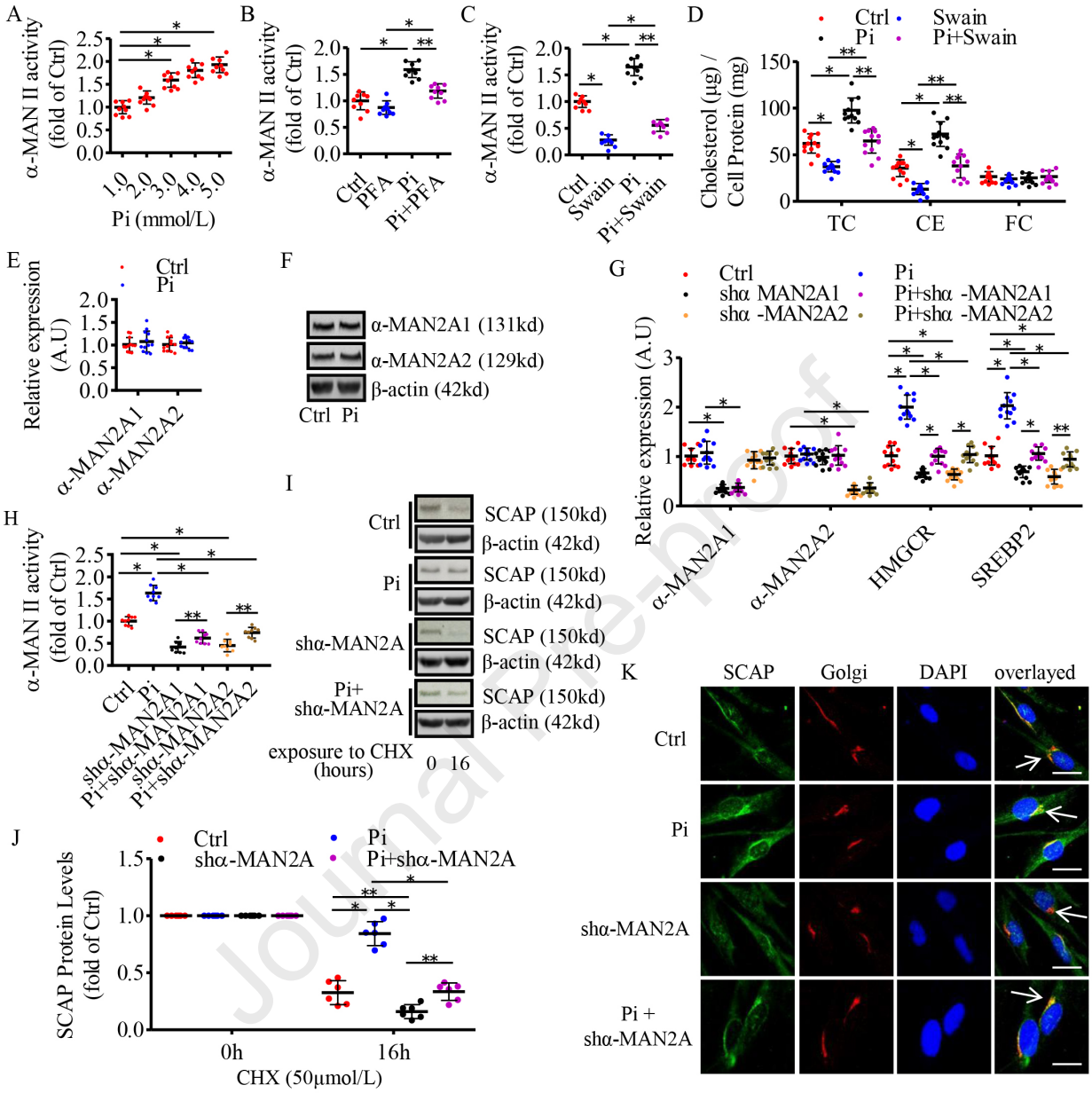

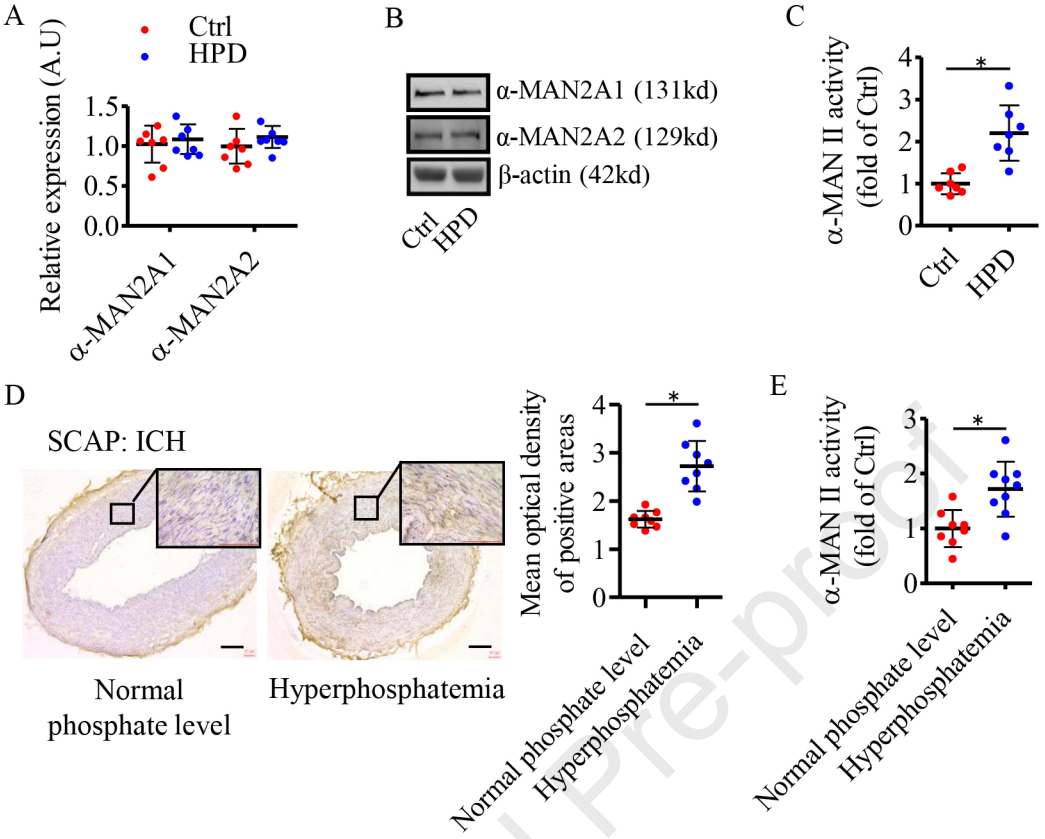

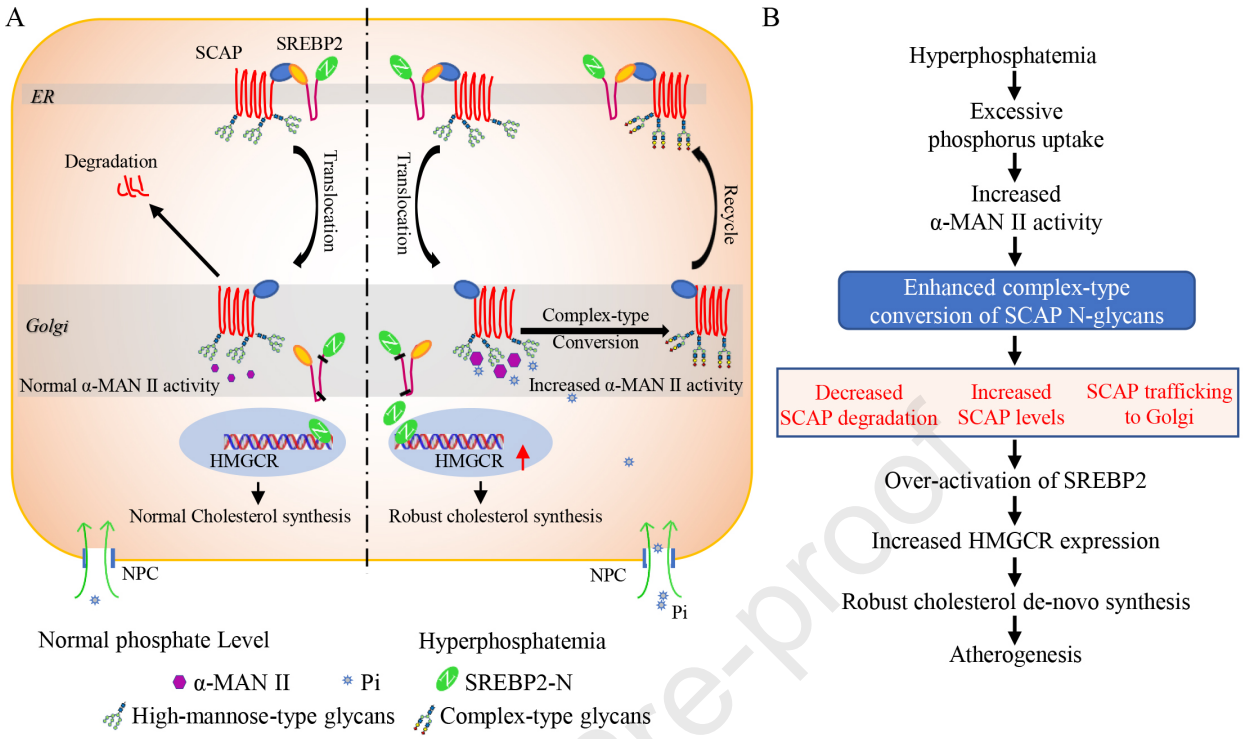

Table 1. Multivariate Logistic Regression Analysis of The Correlation Between Serum P^{3+} level and ASCVD Risk, Stratified by Serum P^{3+} Levels

Item	β value	P value	Odds ratio	95% Confidence interval
Serum P^{3+} levels (mmol/L)		0.001		
1.22~1.46	0.071	0.825	1.073	0.574~2.007
1.47~1.78	0.854	0.010	2.348	1.230~4.481
>1.78	1.057	0.002	2.878	1.479~5.600

Multiple logistic regression models determined with a stepwise procedure, considering all potential predictors and several interactions. Only variables with a significant effect or showing a potentially confounding influence in the model were maintained. P values are for significance between groups.

Supplemental Material

Expanded Methods

1. A cross-sectional study in Chinese CKD population

Briefly, all the participants underwent carotid and femoral B-mode ultrasound imaging to identify the presence of atherosclerotic plaques in the arteries, or coronary CT or angiography examination to make sure the diagnosis of ASCVD. All the subjects were divided into group non-atherosclerosis (non-AS) and group atherosclerosis (AS) according to the presence or absence of atherosclerotic lesions and matched by sex and age (219 cases for each group). Subjects with the sick history of autoimmune disease, primary hyperparathyroidism, familial cardiovascular disease and kidney tumour were excluded.

Related clinical parameters (such as body mass index, (BMI), blood pressure, smoking history, alcohol consumption, diabetes history, dialysis status, et al) and blood biochemical markers (such as serum phosphate, calcium, magnesium, cholesterol, C-reactive protein (CRP), hemoglobin, cardiac troponin I (cTnI), parathyroid hormone, estimated glomerular filtration ratee (eGFR), renal function, type B natriuretic peptide (BNP), serum albumin et al) were collected (Supplemental Table 1).

CKD stage was categorized based on eGFR as determined by the Modification of Diet in Renal Disease Study equation.[1] Null of ASCVD was defined as the absence of a history of coronary artery disease (myocardial infarction, coronary artery bypass graft surgery, or coronary angiography positive), peripheral arterial disease (claudication or vascular bypass surgery) and cerebrovascular disease (stroke), or ultrasound identified atherosclerotic plaque in the peripheral artery. Smoking background included current as well as past history. Diabetes was defined as fasting glucose level more than 7.1 mmol/L or use of hypoglycemic medication. Hypertension was defined as systolic blood pressure ≥140 mmHg, diastolic

blood pressure ≥ 90 mmHg or use of medications prescribed for hypertension. Use of medications was based on clinical prescriptions and confirmed with the patients. All biochemical results were obtained from fasting blood samples.

2. Study animals

When the mice were sacrificed, the blood samples were collected by retro-orbital sampling. Serum was harvested by centrifugation of the blood at 3000rpm for 15 minutes in room temperature and then sent to determine serological markers such as phosphate, calcium, and cholesterol et al. (Supplemental Table 3).

3. Radial artery

Radial artery was discarded artery tissue collected from uremic patients who underwent arteriovenous fistula operation. All procedures were approved by the Ethics Committee for the research of human specimens at Chongqing Medical University. Radial artery ring (3-5mm in length) was stabilized in 10% formalin for 24 hours and then sliced into frozen serial sections. Other fresh radial artery tissues were stored at -80°C for enzyme activity detection.

4. Cell culture

Human aortic VSMCs were obtained from ATCC (USA), and cultured in M199 medium with 20% fetal bovine serum, 2mmol/L L-glutamine, 100U/ml penicillin and 100μg/ml streptomycin. The cells were incubated in M199 containing 2% fetal bovine serum (FBS), 2mmol/L L-glutamine, 100U/ml penicillin, 100μg/ml streptomycin, and antioxidants butylated hydroxytoluene (BHT) and ethylenediaminetetraacetic acid (EDTA) at final concentrations of 20 and 100μmol/L (experimental medium for VSMCs) with treatments for indicated time. Human monocyte cell line (THP-1) (ATCC) was cultured in RPMI 1640 containing 10% FBS, 2mmol/l L-glutamine, 100U/ml penicillin, and 100μg/ml streptomycin. THP-1 was fully differentiated into macrophages by triggered with 160nmol/l phorbol,

12-myristate, 13-acetate (PMA) for 72h in M199 medium with 10% fetal bovine serum, 2mmol/L L-glutamine, 100U/ml penicillin and 100μg/ml streptomycin. Experiments were performed in fresh M199 medium containing 0.2% bovine serum albumin (BSA), 2mmol/l L-glutamine, 100U/ml penicillin, 100μg/ml streptomycin, 20μmol/L BHT and 100μmol/L EDTA (experimental medium for THP-1 macrophages) with treatments for indicated hours. When treated the cells with extra phosphate, the quantity of phosphate already presents in each culture medium was always taken into account. Short hairpin RNA (shRNA) for SREBP2, SCAP, α-mannosidase 2A1 and 2A2 were obtained from Genechem Co., Ltd (Shanghai, China). Phosphonoformic acid (PFA), N-acetylglucosamine (GlcNAc), tunicamycin, swainsonine and other chemicals were purchased from Sigma (USA).

5. Gene transfection

shRNA for SCAP, SREBP2, α-mannosidase 2A1 and 2A2, and their control shRNA (Santa Cruz, USA) were transfected into VSMCs with HiPerFect Transfection Reagent (QIAGEN, Germany) according to the manufacturer's protocol. Cells were kept in growth medium for 24 hours after transfection and then washed twice in PBS before switching onto the experimental medium.

6. ORO staining and morphological examination

2×10^5 VSMCs seeded in 8-well chamber slides (Becton Dickinson, Oxford, UK) were incubated in experimental medium for 24 hours. 2×10^5 THP-1 cells were differentiated into macrophages before transferred into fresh experimental medium for 24 hours. Then the cells were switched to fresh experimental medium in the absence or presence of 3.0mmol/L phosphate. After 24 hours incubation, the cells were washed 3 times in PBS, and stained by Oil Red O (ORO) as we described previously.[2] The longitudinal dissection of the aortic tissue and aortic root frozen serial sections of the ApoE-/- mice were recovered to room temperature, then washed 3 times in PBS, stained and counterstained followed the same steps as the cells

were treated. Finally, the cells and aortic root tissue were examined by light microscopy (Olympus, Japan). Semi-quantitative analysis of ORO positive staining was performed by the Image-J software.

7. Examination of Dil-LDL uptake

VSMCs planted in 8-well chamber slides or 6-well plates were cultured in experimental medium with or with excessive phosphate (3.0mmol/L) for 24 hours, then switched onto fresh medium with 25μmol/L Dil-LDL for 4 hours. Treated cells in chamber slides were extensively washed with PBS for 3 times before fixed with 4% paraformaldehyde for 20 minutes in room temperature. Then the slides were covered with DAPI mounting medium, and the cells were examined with a fluorescence microscope (Olympus, Japan). Treated cells in 6-well plates were harvested for protein extraction as usual, and protein aliquots were applied for Dil-LDL quantification using a standard curve and normalized by total protein from cells.

8. Total RNA isolation and Real-time quantitative PCR

Total RNA was isolated from cultured cells using TRIzol (Ambion, UK) or from artery tissue using RNeasy Fibrous Tissue Mini Kit (Qiagen, German). Total RNA (1μg) was used as a template for reverse transcription with a High Capacity cDNA RT Kit from ABI (Applied Biosystems, UK). Real-time qPCR was performed in an ABI 7000 Sequence Detection System using SYBR Green dye according to the manufacturer's instruction (Applied Biosystems, UK) as we described previously.[2] All the Taqman primers were designed by Primer Express Software V3.0 (Supplemental Table 5 and 6).

9. Protein isolation and Western-blotting

Identical amounts of protein from cell extracts or nuclear extracts of cultured cells or artery tissue were denatured and then subjected to electrophoresis on an 8% SDS polyacrylamide gel and electrophoretic transfer to a nitrocellulose membrane as we described

before.[2] Rabbit anti-human/mouse antibody for HMGCR (Abcam, UK), SCAP (Abcam, UK), ABCA1 (Abcam, UK), LXRα (Abcam, UK), α-mannosidase 2A2 (Abcam, UK), or mouse anti-human/mouse antibody for SREBP2 (Santa Cruz, USA), lamin A (Santa Cruz, USA), α-mannosidase 2A1 (Santa Cruz, USA), β-actin (Sigma, USA), or chicken anti-human/mouse antibody for LDLr (Abcam, UK) were used as the primary antibodies. A rabbit anti-mouse or goat anti-rabbit and goat anti chicken HRP-labeled antibody (Abcam, UK) was used as the secondary antibodies. Semi-quantitative analysis of Western blots was performed by the Image-J software.

10. Immunohistochemistry staining

The aortic root frozen serial sections of the ApoE-/- mice and radial artery sections of uremic patients were recovered to room temperature, washed 3 times in PBS, fixed by acetone for 30minutes, and dehydrated by gradient alcohol (70%, 80%, 90%, 95%). The activity of endogenous peroxidase was eliminated by 3% H_2O_2 for 30minutes, followed by transmembrane treatment with 0.4% Triton X-100 for 15minutes and blocked by 10% goat serum for 1hour. Then the serum was removed, and the sections were incubated with rabbit anti-human/mouse SCAP antibody (Santa Cruz, USA) (using PBS as an alternative for the negative control sections) overnight at 4°C. The next day, sections were washed for 3 times in PBS, and then incubated in HRP-labeled goat anti-rabbit secondary antibody for 30minutes at 37°C. Then the sections were washed for 3 times in PBS, reacted with DAB solution for 5 to 10seconds, then the reaction was terminated by tap water washing for 5minutes and counterstained by hematoxylin for 3minutes. Finally, the artery tissues were examined by light microscopy (Olympus, Japan). Semi-quantitative analysis was performed by the software of Image-Pro Plus version 5.0.

11. Intracellular Cholesterol quantification

1.0×10^6 VSMCs or THP-1 macrophages planted in 6-well plates were cultured in

experimental medium for 24hours, then switched to the fresh experimental medium in the absence or presence of different treatments. 24hours later, cells were washed twice in PBS. Intracellular lipids were extracted in chloroform/methanol (2:1) and dried under vacuum, then the total cholesterol (TC) and free cholesterol (FC) content were measured by an enzymatic assay normalized by total cell proteins as described previously.[2] The concentration of cholesterol ester (CE) was calculated using TC minus FC.

12. Confocal microscopy

Cells were cultured in chamber slides in experimental medium with indicated treatments for 24hours. After 24hours incubation, the cells were dual stained as previously described.[2] The rabbit polyclonal anti-human SCAP antibody produced by immunizing rabbits with the synthetic peptide PVDSDRKQGEPTEQC in our laboratory and mouse anti-Golgi antibody (Molecular Probes, UK) were used as the primary antibodies, goat anti-rabbit Fluor (green) 488 for SCAP and goat anti-mouse Fluor (red) 594 for Golgi (Molecular Probes, USA) were used as the secondary antibodies. Finally, the cells were examined with a confocal microscope (Olympus, Japan).

Additional Figures

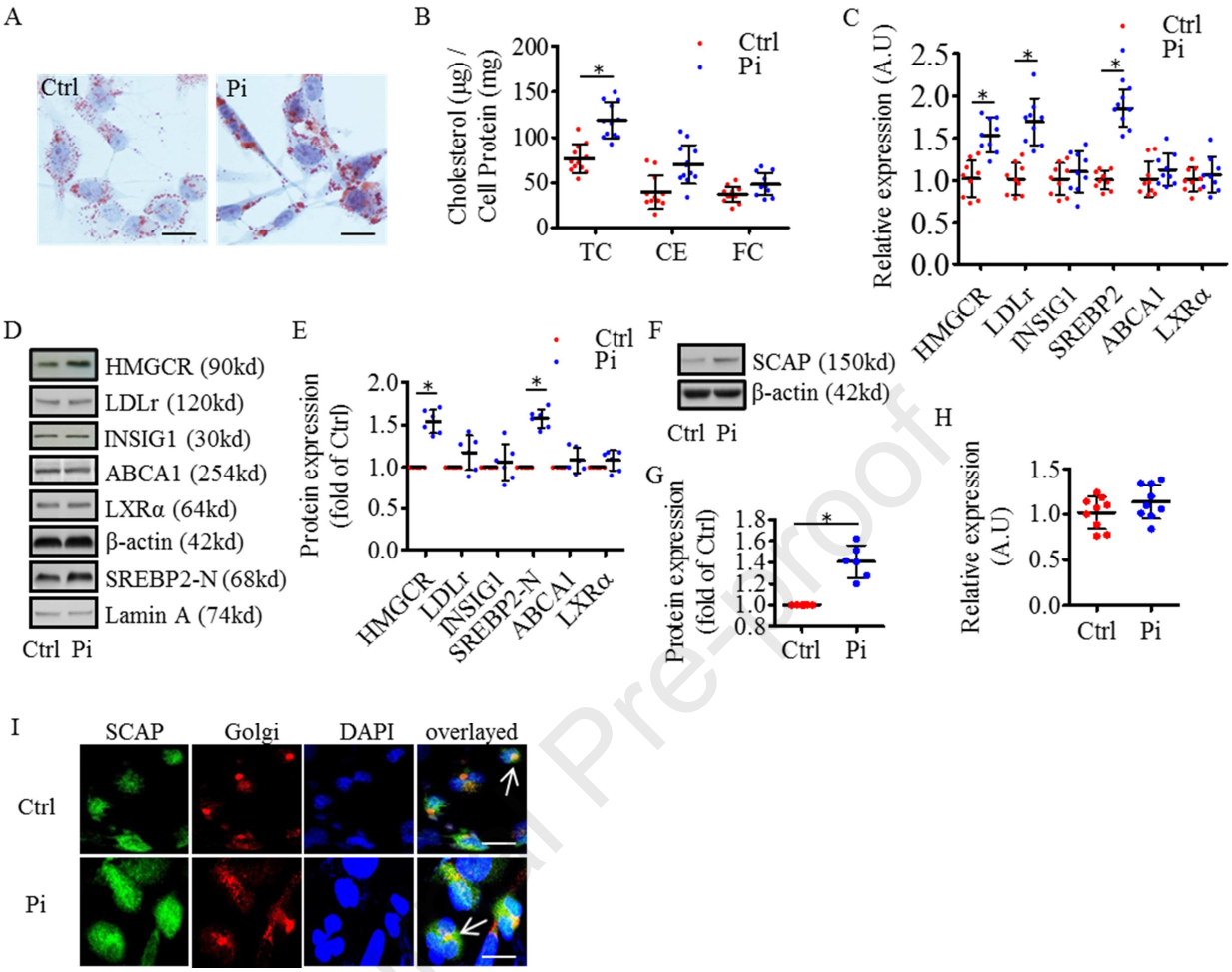

Supplemental Figure 1. Excess phosphate induced translocation of SCAP and cholesterol accumulation in THP-1 macrophages. The THP-1 macrophages were cultured in experimental medium with or without excess phosphate for 24 hours. (A) The intracellular neutral lipids stained by ORO. The results are typical of those observed in four separate experiments. Scale bar=50μm. (B) Quantification of intracellular free cholesterol (FC) and cholesterol ester (CE). Values are means ±SEM from 3 experimental repeats (n=12 per group). (C and H) The gene expressions of the cholesterol metabolic components determined by Real-time PCR. β-Actin served as the reference gene. Values are means ±SEM from 3

experimental repeats (n=9 per group). (D and F) The protein levels of the cholesterol metabolic components examined by Western blotting. The demonstrated bands were typical from 3 experimental repeats. β-Actin served as the domestic control for the cytoplasmic protein, and lamin A served as the reference for the nuclear protein. (E and G) The densitometric scans of protein bands represented by means ±SD from 3 experimental repeats (n=6 per group), normalized by comparison with reference protein and expressed as fold of control. (I) The colocalization of SCAP with Golgi apparatus observed by confocal microscopy (as arrow pointed). The results are typical of those observed in four separate experiments. Scale bar=50μm. Statistical significance was assessed using 2-tailed Student' s t-test in B, C, E, G and H. * $P<0.01$. Pi, excess phosphate.

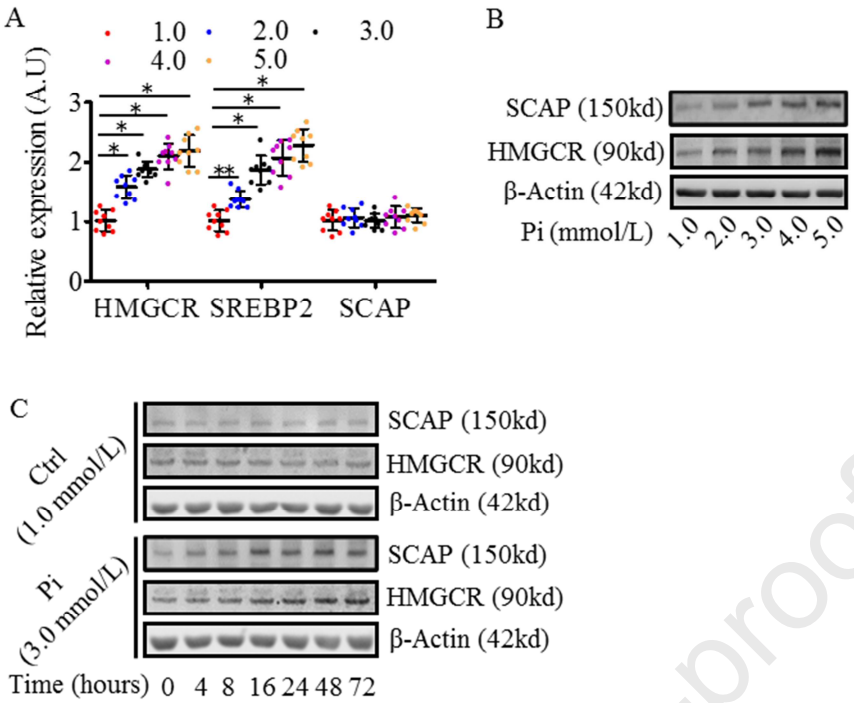

Supplemental Figure 2. The dose response and time-course effect of excess phosphate on SCAP-SREBP2 signaling. (A)-(B) The VSMCs were cultured in experimental medium with different concentrations of phosphate from 1.0 to 5.0 mmol/L for 24 hours. (C) The VSMCs were cultured in experimental medium with or without excess phosphate (3.0mmol/L) for the indicated time. (A) The gene expression determined by Real-time PCR. β-Actin served as the reference gene. Values are means ±SD from 3 experimental repeats (n=9). (B and C) The protein levels examined by Western blotting. The demonstrated bands were typical from 3 experimental repeats, β-actin served as the reference. * P<0.01. Pi, excess phosphate.

Additional Tables

Supplemental Table 1. Comparison of The Basic Characteristics Between AS and Non-AS Groups

Characteristic	Non-AS group (n=219)	AS group (n=219)	*P* value
BMI (kg/m^2)	23.02±2.97	22.79±2.99	0.419
Hypertension (n, %)	173 (79.00)	194 (88.60)	0.006
SBP (mmHg)	150.85±25.12	152.74±25.50	0.436
Taking antihypertensive drugs (n, %)	150 (68.5)	176 (34.7)	0.182
Diabetes (n, %)	69 (31.50)	107 (48.90)	<0.001
Good glycemic control (n, %)	52 (23.70)	90 (41.10)	<0.001
eGFR ($ml/(min.1.73m^2)$)	11.6 (8.73-27)	9.77 (7.89-13)	<0.001
Maintenance hemodialysis (n, %)	113 (51.60)	149 (68.00)	<0.001
Smoking (n, %)	86 (39.30)	105 (47.90)	0.067
Current smoking (n, %)	47 (21.50)	52 (23.70)	0.568
Alcohol consumption (n, %)	56 (25.60)	60 (27.40)	0.665
Hemoglobin (g/L)	97.73±24.84	100.16±25.50	0.320
Serum Ca^{2+} (mmol/L)	2.16 (2.01-2.29)	2.15 (1.99-2.31)	0.988
Serum Mg^{2+} (mmol/L)	0.90 (0.81-1.00)	0.94 (0.84-1.07)	0.005
Serum Pi^{3+} (mmol/L)	1.36 (1.16-1.66)	1.60 (1.31-1.94)	<0.001
Taking phosphate lowering drugs (n, %)	63 (28.80)	76 (34.70)	0.182
Parathyroid hormone (pg/ml)	213.40 (106.70-357.90)	196.25 (96.93-361.25)	0.817
TC (mmol/L)	4.03±1.23	3.88±1.20	0.233
HDL (mmol/L)	1.19±1.02	1.09±0.36	0.195

LDL (mmol/L)	2.32 (1.81-3.03)	2.23 (1.60-2.87)	0.169
Apolipoprotein A1 (g/L)	1.20±0.33	1.20±0.28	0.782
Apolipoprotein B (g/L)	0.77 (0.63-0.98)	0.73 (0.56-0.94)	0.225
Lipoprotein (a) (mg/L)	184.00 (84.50-439.00)	208.00 (93.00-495.00)	0.312
Triglycerides (mmol/L)	1.28 (0.89-1.93)	1.19 (0.84-1.84)	0.499
Serum albumin (g/L)	35(32-38)	36(33-39)	0.044
BNP (pg/ml)	4443(797.5-9253)	5633(2207-115202.5)	0.007
Myoglobin (μg/L)	135.15 (88.23-225.10)	178.05 (114.75-272.40)	0.001
CK-MB (μg/L)	2.15 (1.20-3.48)	2.00 (1.30-3.90)	0.311
cTnI (μg/L)	0.05 (0.02-0.08)	0.07 (0.03-0.12)	0.001
CRP (mg/L)	4.41(1.25-20)	4.195(0.9275-20)	0.497

Abbreviations: BMI. Body mass index; SBP. Systolic blood pressure; TC. Total cholesterol; HDL. High density lipoprotein; LDL. Low density lipoprotein. CK-MB. Creatine kinase-MB; cTnI. Cardiac troponin I.

Supplemental Table 2. The Univariate Logistic Regression Analysis of Vascular Risk Factors Between AS and Non-AS Groups

Risk factors	β value	P value	Odds ratio	95% Confidence interval
BMI	-0.026	0.418	0.974	0.915~1.038
Hypertension	0.724	0.007	2.063	1.216~3.500
SBP	0.003	0.435	1.003	0.996~1.010
Taking antihypertensive drugs	0.633	0.005	1.883	1.214~2.920
Diabetes	0.731	<0.001	2.077	1.407~3.065
Good glycemic control	0.807	<0.001	2.241	1.485~3.381
eGFR	-0.022	<0.001	0.978	0.968-0.988
Maintenance hemodialysis	0.692	<0.001	1.997	1.354~2.945
Smoking	0.354	0.068	1.424	0.975~2.081
Current smoking	0.131	0.568	1.140	0.728~1.784
Alcohol consumption	0.094	0.665	1.098	0.718~1.680
Hemoglobin	0.004	0.319	1.004	0.996~1.012
Serum Ca^{2+}	0.002	0.995	1.002	0.529~1.900
Serum Mg^{2+}	1.875	0.002	6.523	2.037~20.892
TC	-0.100	0.233	0.905	0.768~1.066
HDL	-0.252	0.250	0.778	0.506~1.194
LDL	-0.102	0.310	0.903	0.741~1.100
Apolipoprotein A1	-0.093	0.781	0.911	0.472~1.757
Apolipoprotein B	-0.158	0.657	0.854	0.427~1.711
Lipoprotein (a)	0.000	0.392	1.000	1.000~1.001

Triglycerides	0.005	0.953	1.005	0.859~1.174
Serum albumin	0.036	0.096	1.037	0.994-1.081
BNP	0.000	0.076	1.000	1.000-1.000
Myoglobin	0.000	0.432	1.000	1.000~1.001
CK-MB	0.078	0.034	1.082	1.006~1.163
cTnI	0.000	0.554	1.000	1.000~1.000
CRP	0.003	0.808	1.003	0.979-1.028
Parathyroid hormone	0.000	0.535	1.000	0.999~1.000
Phosphate lowering drugs	0.275	0.183	1.316	0.879~1.971
Serum Pi^{3+}	0.806	<0.001	2.239	1.526~3.285
Serum phosphorus levels (mmol/L)		<0.001		
1.22~1.46	0.330	0.239	1.392	0.802~2.413
1.47~1.78	1.197	<0.001	3.311	1.889~5.805
>1.78	1.360	<0.001	3.898	2.219~6.848

Abbreviations: BMI. Body mass index; SBP. Systolic blood pressure; TC. Total cholesterol; HDL. High density lipoprotein; LDL. Low density lipoprotein. CK-MB. Creatine kinase-MB; cTnI. Cardiac troponin I.

Supplemental Table 3. Basic Characteristics of Normal Chow and High Phosphate Diet Fed Apo E-/- Mice When Sacrificed

Items, unit	Normal chow	High phosphate diet
Body weight, g	32.03±2.31	32.09±2.41
Serum Pi^{3+}, mmol/L	2.14±0.09	2.68±0.27*
Serum Ca^{2+}, mmol/L	2.56±0.26	2.56±0.20
Serum Mg^{2+}, mmol/L	1.35±0.09	1.39±0.14
Parathyroid hormone, ng/L	64.93±21.83	91.01±17.12*
Triglycerides, mmol/L	1.50±0.39	1.53±0.33
TC, mmol/L	13.03±2.01	13.17±3.10
LDL, mmol/L	1.39±0.44	1.42±0.37
HDL, mmol/L	0.50±0.09	0.57±0.11
Glucose, mmol/L	10.59±1.53	10.83±3.26
ALT, IU/L	38.5±6.7	48.25±28.17
AST, IU/L	121.13±64.7	112.88±37.6
Albumin, g/L	29.2±1.53	28.06±1.55
Blood Urea nitrogen, mmol/L	11.84±1.21	11.61±2.08
Creatinine, μmol/L	22.8±11.08	23.06±6.28
CRP, mg/L	0.04±0.03	0.04±0.03

Supplemental Table 4. The Formula of The Main Nutrition Gradients in Normal Chow and High Phosphate Diet

Ingredients	Phosphate	Calcium	Protein	Carbohydrate	Fat	Fibre
Normal chow	0.60%	1.70%	20.60%	75%	4.40%	7.70%
High phosphate diet	1.60%	1.70%	20.60%	75%	4.40%	7.70%

Supplemental Table 5. Mouse TaqMan Primers for Real-time PCR

Genes	Primers
LDLr	Forward: 5'-CTGTGGGCTCCATAGGCTATCT-3'
	Reverse: 5'-GCGGTCCAGGGTCATCTTC-3'
HMGCR	Forward: 5'-CCTGGGCCCCACATTCA-3'
	Reverse: 5'-GACATGGTGCCAACTCCAATC-3'
INSIG1	Forward: 5′-ACGCCAGTGCCAAATTAGAT-3′
	Reverse: 5′-CTTCGGGAACGATCAAATG-3′
SREBP2	Forward: 5'-GCGCCAGGAGAACATGGT-3'
	Reverse: 5'-CGATGCCCTTCAGGAGCTT-3'
SCAP	Forward: 5'-ACTGGACTGAAGGCAGGTCAA-3'
	Reverse: 5'-GCCTCTAGTCTAGGTCCAAAGAGTTG-3'
ABCA1	Forward: 5'-ACTTAGGGCACAATTCCACAAGA-3'
	Reverse: 5'-CTCCTGTGGTGTTTCTGGATGA-3'
LXRα	Forward: 5'-GGAGTGTCGACTTCGCAAATG-3'
	Reverse: 5'-TCAAGCGGATCTGTTCTTCTGA-3'
α-MAN 2A1	Forward: 5'-TCGCTGAGAACAACGAGATCATCT-3'
	Reverse: 5'-GTGAAGCAAACAAACAGTC-3'
α-MAN 2A2	Forward: 5'-ACAACATCAGTGCCCAAAAGAG-3'
	Reverse: 5'-TGAGCTGGTCAACCAAGGCAAAGT-3'
β-actin	Forward: 5'-ACGGCCAGGTCATCACTATTG-3'
	Reverse: 5'-CACAGGATTCCATACCCAAGAAG-3'

Supplemental Table 6. Human TaqMan Primers for Real-time PCR

Genes	Primers
LDLr	Forward: 5'-GTGTCACAGCGGCGAATG-3'
	Reverse: 5'-CGCACTCTTTGATGGGTTCA-3'
HMGCR	Forward: 5'-TCTGGCAGTCAGTGGGAACTATT-3'
	Reverse: 5'-CCTCGTCCTTCGATCCAATTT-3'
INSIG1	Forward:5'-TGCAGATCCAGAGGAATGTCAC-3′
	Reverse:5'-CCAGGCGGAGGAAAAGATG-3′
SREBP2	Forward: 5'-CGATGCCCTTCAGGAGCTT-3'
	Reverse: 5'-GCGCCAGGAGAACATGGT-3'
SCAP	Forward: 5'-GGGAACTTCTGGCAGAATGACT-3'
	Reverse: 5'-CTGGTGGATGGTCCCAATG-3'
ABCA1	Forward: 5'-GCAGCAGAGCGAGTACTTCGTT-3'
	Reverse: 5'-CAAGACTATGCAGCAATGTTTTTGT-3'
LXRα	Forward: 5'-AGAAGAACAGATCCGCCTGAAG-3'
	Reverse: 5'-GGCAAGGATGTGGCATGAG-3'
α-MAN 2A1	Forward: 5'-TATGCCTGATGAAGCTACTCCACA -3'
	Reverse: 5'-ATAAGCCATTGTTGGTGAGTGTCC-3'
α-MAN 2A2	Forward: 5'-TGTGTCGGAGGAGCTGCCGTTT-3'
	Reverse: 5'-TCTTGATCCAGCCTGGGTCAT-3'
β-actin	Forward: 5'-CCTGGCACCCAGCACAAT-3'
	Reverse: 5'-GCCGATCCACACGGAGTACT-3'

Reference

1. Levey AS, Bosch JP, Lewis JB, et al. A more accurate method to estimate glomerular filtration rate from serum creatinine: a new prediction equation. Ann. Intern Med. 1999; 130:461-70.

2. Chen Y, Ku H, Zhao L, et al. Inflammatory stress induces statin resistance by disrupting 3-hydroxy-3-methylglutaryl-CoA reductase feedback regulation. Arterioscler Thromb Vasc Biol. 2014; 34:365-376